

All-optical spin locking in alkali-metal-vapor magnetometers

Guzhi Bao^{1,2}, Dimitra Kanta², Dionysios Antypas³, Simon Rochester⁴, Kasper Jensen⁵, Weiping Zhang^{1,6,7}, Arne Wickenbrock², and Dmitry Budker^{2,3,8,9}

¹*School of Physics and Astronomy, Shanghai Jiao Tong University, and Tsung-Dao Lee Institute, Shanghai 200240, China*

²*Johannes Gutenberg-Universität Mainz, 55128 Mainz, Germany*

³*Helmholtz Institut Mainz, 55099 Mainz, Germany*

⁴*Rochester Scientific, LLC., El Cerrito, California 94530, USA*

⁵*School of Physics and Astronomy, University of Nottingham, University Park, Nottingham NG7 2RD, United Kingdom*

⁶*Collaborative Innovation Center of Extreme Optics, Shanxi University, Taiyuan, Shanxi 030006, China*

⁷*Shanghai Research Center for Quantum Sciences, Shanghai 201315, People's Republic of China*

⁸*Department of Physics, University of California, Berkeley, California 94720-7300, USA*

⁹*Nuclear Science Division, Lawrence Berkeley National Laboratory, Berkeley, California 94720, USA*

The nonlinear Zeeman effect can induce splittings and asymmetries of magnetic-resonance lines in the geophysical magnetic-field range. We demonstrate an all-optical scheme, based on spin locking, to suppress the nonlinear Zeeman effect. This scheme achieves spin locking via an effective oscillating magnetic field in the form of AC Stark shifts induced by an intensity- and polarization-modulated laser beam. This results in the collapse of the multi-component asymmetric magnetic-resonance line with ~ 100 Hz width in the Earth-field range into a peak with a central component width of 25 Hz. The technique is expected to be broadly applicable in practical magnetometry, potentially boosting the sensitivity and accuracy of Earth-surveying magnetometers by increasing the magnetic-resonance amplitude and decreasing its width. An advantage of the all-optical approach is the absence of cross-talk between nearby sensors when they are used in a gradiometric or array arrangement.

I. INTRODUCTION

Measurements of magnetic fields with femtotesla sensitivity are critical to many applications, including geophysics [1], fundamental physics [2, 3], and medicine [4–7]. Optical magnetometers [8–11] currently reach subfemtotesla/ $\sqrt{\text{Hz}}$ sensitivity levels for submicrotesla fields [1]. However, in the geophysical field range (up to 100 μT), the main limitation to the magnetic-resonance line width and sensitivity is the nonlinear Zeeman (NLZ) splitting [12–16]. The NLZ effect can cause splitting of resonance components, leading to a decrease in magnetometer signal and to the spurious dependence of scalar-sensor readings on the relative orientation of sensor and magnetic field. NLZ shifts can be effectively canceled by means of several techniques, including the use of double-modulated synchronous optical pumping [13], high-order polarization moments [14], and tensor light-shift effects [15, 17]. Recently, a new scheme to suppress the NLZ effect by adding a so-called spin-locking field [18] was demonstrated. In this scheme, an oscillating magnetic field (RF field) or short magnetic-field pulses applied in the laboratory frame results in an effective static magnetic field along the atomic magnetization in the rotating frame. The atomic spin state then precesses about this static field, rather than evolving into a different state, as it would under the action of the nonlinear Zeeman effect alone. As a result, this spin-locking field prevents splitting, shifts, and line-shape asymmetries from occurring. A potential drawback to this approach is that globally applied magnetic fields may lead to crosstalk between

closely located sensors (as in a gradiometer); this would limit the applicability of this technique to sensor networks, which are important in biomedical applications, such as imaging the human heart or mapping brain activity [4, 19–22], as well as fundamental physics applications. Additionally, in remote magnetometry applications, spin-locking magnetic fields cannot be directly applied to the atomic sample [23–25].

To circumvent these difficulties, spin locking can be induced using a fictitious magnetic field—in the form of a light field—rather than a real magnetic field. In the presence of light, the energies of Zeeman sublevels are subject to AC Stark shifts, or “light shifts” [26–29]. There are, depending on the polarization of the light and the atomic transition, scalar, vector, and tensor shifts. In particular, the effect of the vector light shift (VLS) is analogous to a fictitious magnetic field [27, 30]. VLS have been studied in the context of all-optical magnetometry [8, 29, 31]; in particular, light was used to substitute for RF fields [32, 33]. Here, we demonstrate all-optical compensation of the nonlinear Zeeman shift in a magnetometer using spin locking by replacing the RF field with an intensity- and polarization-modulated laser beam. This method allows for the building of a highly sensitive multi-sensor magnetometer array capable of working in the magnetic-field range of the Earth.

II. THEORETICAL DESCRIPTION

A. Nonlinear Zeeman effect

The ground-state Hamiltonian for an atom in a magnetic field for states with electronic angular momentum $J = 1/2$, including both the hyperfine and Zeeman interactions, is

$$\hat{H} = A_J \mathbf{I} \cdot \mathbf{J} + g_s \mu_B \mathbf{S} \cdot \mathbf{B} - g_I \mu_N \mathbf{I} \cdot \mathbf{B}, \quad (1)$$

where A_J is the hyperfine coupling constant, g_s and g_I are respectively the electron-spin and nuclear Landé factors of the atom, I is the nuclear spin, μ_B is the Bohr magneton, and μ_N is the nuclear magneton. The first term describes the hyperfine interaction and the second and third terms describe Zeeman interactions. For a system with one valence electron in an $S(J = 1/2)$ level, the analytical solution for the eigenvalues of the Hamiltonian is given by the Breit-Rabi formula, which provides the energy shifts of the magnetic sublevels $|m\rangle$ for a state with a total angular momentum F in a magnetic field of strength B [31, 34]:

$$E_m = \frac{\Delta_{hf}}{2(2I+1)} - g_I \mu_B m B \pm \frac{\Delta_{hf}}{2} \left(1 + \frac{4m\xi}{2I+1} + \xi^2 \right)^{1/2}, \quad (2)$$

where $\xi = (g_J + g_I) \mu_B B / \Delta_{hf}$, Δ_{hf} is the hyperfine-structure interval and the \pm sign refers to the $F = I \pm 1/2$ hyperfine levels. While the nonlinear term in Eq. (2) can be neglected for low-field magnetometry, it is important under Earth's magnetic field. Expanding the eigenenergies as a series in B around zero, the transition frequencies corresponding to $\Delta m = 1$ for the cesium $6^2S_{1/2} F = 4$ system are

$$E_{m+1} - E_m \approx \frac{\mu_B B}{4} + \frac{(\mu_B B)^2}{16 \Delta_{hf}} (2m - 1), \quad (3)$$

where $\omega_{rev} = (\mu_B B)^2 / 16 \hbar \Delta_{hf}$ is the so-called quantum-beat revival frequency [13], $g_J \approx 2$ and we neglect the Zeeman energy of the nuclear spin [last term in Eq. (1)] as $\mu_N \ll \mu_B$. Assuming an Earth-range magnetic field of 50 μ T, the calculated revival frequency is $\omega_{rev} = 2\pi \cdot 3.3$ Hz [31]. This frequency is comparable to the magnetic resonance width and hence the system is strongly affected by the nonlinear Zeeman effect. The Cs magnetic resonance is split into eight peaks (see Fig. 4), broadening the line width, reducing the signal amplitude, and reducing magnetometer sensitivity.

B. Spin locking

To describe the physics of spin locking, we start with a total angular momentum $F = 1$ system interacting with a leading magnetic field along $\hat{\mathbf{z}}$ and an RF field along $\hat{\mathbf{x}}$. The Hamiltonian for the system is modelled as:

$$\hat{H} = \hbar[\Omega_L F_z + \omega_{rev} F_z^2 + \Omega_{rf} \cos(\omega_{rf} t) F_x], \quad (4)$$

where Ω_L is the Larmor frequency of leading magnetic field, ω_{rev} is the ‘‘revival’’ frequency characterizing the strength of the NLZ effect; Ω_{rf} is the Larmor frequency induced by the oscillating field and proportional to its amplitude, ω_{rf} is the oscillation frequency of oscillating magnetic field.

The atomic spins are initially prepared in the $m_F = 1$ state along the $\hat{\mathbf{x}}$ direction by a circularly polarized pump field, and we assume that the probe-light power is sufficiently low to be neglected for the dynamics. With the quantization axis along $\hat{\mathbf{z}}$, the initial state is

$$\psi(0) = \frac{1}{2} \begin{pmatrix} 1 \\ \sqrt{2} \\ 1 \end{pmatrix}. \quad (5)$$

The Hamiltonian for the system under the rotating-wave approximation (RWA) for the RF field with $\Omega_L = \omega_{rf}$ is [18]

$$\hat{H}_{RWA} = \hbar \begin{pmatrix} \omega_{rev} & -\frac{\Omega_{rf}}{2\sqrt{2}} & 0 \\ -\frac{\Omega_{rf}}{2\sqrt{2}} & 0 & -\frac{\Omega_{rf}}{2\sqrt{2}} \\ 0 & -\frac{\Omega_{rf}}{2\sqrt{2}} & \omega_{rev} \end{pmatrix}, \quad (6)$$

With this Hamiltonian, the energy eigenvalues and energy eigenstates are:

$$\begin{aligned} E_1 &= \hbar \omega_{rev}, & \Psi_1 &= \begin{pmatrix} -1 \\ 0 \\ 1 \end{pmatrix}, \\ E_2 &= \frac{\hbar}{2}(\omega_{rev} - \omega_l), & \Psi_2 &= \begin{pmatrix} 1 \\ \frac{\sqrt{2}}{\Omega_{rf}}(\omega_{rev} + \omega_l) \\ 1 \end{pmatrix}, \\ E_3 &= \frac{\hbar}{2}(\omega_{rev} + \omega_l), & \Psi_3 &= \begin{pmatrix} 1 \\ \frac{\sqrt{2}}{\Omega_{rf}}(\omega_{rev} - \omega_l) \\ 1 \end{pmatrix}, \end{aligned} \quad (7)$$

where $\omega_l = (\omega_{rev}^2 + \Omega_{rf}^2)^{1/2}$ is the spin-locking oscillation frequency. The eigenstates are not normalized. We write the state $\psi(t)$ of F as a superposition of energy eigenstates Ψ_k with eigenvalues E_k :

$$\psi(t) = \sum_k \Psi_k e^{-iE_k t / \hbar}. \quad (8)$$

The probability $P(t, 0)$ for an atom to be found in the initial state, $|\langle \psi(t) | \psi(0) \rangle|^2$, can be written as

$$P(t, 0) = \frac{\omega_l^2 + \Omega_{rf}^2 + \omega_{rev}^2 \cos(\omega_l t)}{2\omega_l^2}, \quad (9)$$

With an increase in the spin-locking field amplitude, the oscillating component of $P(t, 0)$ decreases in amplitude and the frequency of the oscillation increases (see Fig. 1). In this simplified model, it appears that spin locking improves with the amplitude of the applied field. The calculations mentioned above are performed under the RWA.

When the RF field is large enough so that the RWA is not valid ($\Omega_{rf} \approx \omega_{rev}$), the presence of the locking field leads to power broadening of the magnetic resonance; under this condition the optimal amplitude of the field is such that Ω_{rf} is comparable to ω_{rev} .

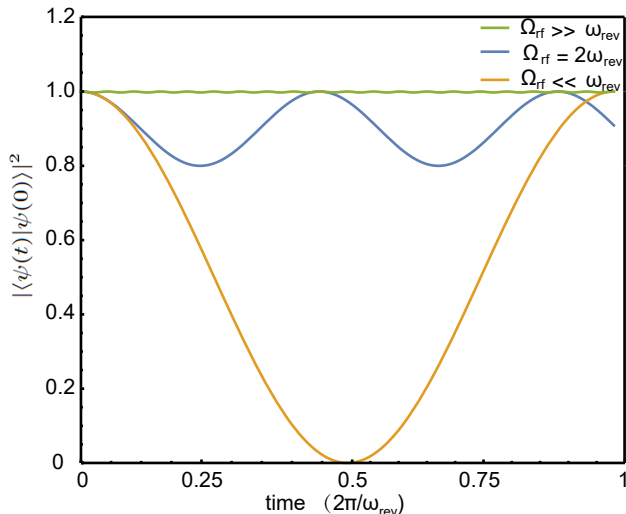


FIG. 1. Probability $P(t,0)$ for an atom to be found in the initial state. For small amplitudes of the spin-locking field ($\Omega_{rf} \ll \omega_{rev}$), the probability undergoes quantum beating. If the amplitude of the spin-locking field is much larger than the NLZ parameter ($\Omega_{rf} \gg \omega_{rev}$), the atoms remain in the initial state. If the amplitude of the spin-locking field is equal to the NLZ parameter ($\Omega_{rf} = 2\omega_{rev}$), the atoms are partially locked in the initial state and the populations undergo oscillation with frequency ω_l .

C. Spin Locking with AC Stark shift

The vector component of the light shift induced by circularly polarized light can be interpreted as a fictitious magnetic field along the light propagation direction, with magnitude [35]

$$B_{\text{fict}} = \frac{-c(\Delta)\mathcal{I}\epsilon}{\hbar\gamma_{\text{Cs}}}, \quad (10)$$

where $c(\Delta)$ is a proportionality constant that depends on atomic parameters and the frequency detuning Δ from atomic resonance, \mathcal{I} is the light intensity, $\gamma_{\text{Cs}} = 2.2 \cdot 10^{10}$ rad/(s · T) is the cesium gyromagnetic ratio and $\epsilon = [\mathcal{I}(\sigma_+) - \mathcal{I}(\sigma_-)]/\mathcal{I}$ is the Stokes parameter specifying the degree of circular light polarization ($\epsilon = +1$ for σ_+ -polarized light, $\epsilon = -1$ for σ_- -polarized light and $\epsilon = 0$ for linear polarization).

Consider the same system as in the previous section—an $F = 1$ system with a leading magnetic field along \hat{z} and a circularly polarized pump beam propagating along \hat{x} . Now, rather than an RF field, we apply a modulated,

circularly polarized light beam propagating in the same direction as the pump, near-resonant with a transition to a $F = 0$ state, in order to induce vector light shifts. The effective Stark-shift Hamiltonian (see Appendix A) for σ_+ and σ_- beam can be represented as

$$\begin{aligned} \hat{H}_{eff}^+ &= \hbar \frac{(\Omega_{LS}^+)^2}{\Delta} (K_1 - K_2), \\ \hat{H}_{eff}^- &= \hbar \frac{(\Omega_{LS}^-)^2}{\Delta} (K_1 + K_2), \\ K_1 &= \frac{1}{48} \begin{pmatrix} 1 & 0 & 1 \\ 0 & 2 & 0 \\ 1 & 0 & 1 \end{pmatrix}, \\ K_2 &= \frac{1}{48} \begin{pmatrix} 0 & \sqrt{2} & 0 \\ \sqrt{2} & 0 & \sqrt{2} \\ 0 & \sqrt{2} & 0 \end{pmatrix}, \end{aligned} \quad (11)$$

where Ω_{LS}^\pm is the Rabi frequency of σ_\pm -polarized light, $|\Omega_{LS}^\pm|^2$ is proportional to the intensity of the light $\mathcal{I}(\sigma_\pm)$, and Δ is the detuning. The light-shift beam can be intensity- and/or polarization-modulated (see the details in the experimental section below). The intensity of σ_\pm -polarized light in Fig. 4(c) is:

$$\begin{aligned} \mathcal{I}(\sigma_-) &= I_0 \frac{\cos(\omega_{rf} t) + |\cos(\omega_{rf} t)|}{2}, \\ \mathcal{I}(\sigma_+) &= I_0 \frac{-\cos(\omega_{rf} t) + |\cos(\omega_{rf} t)|}{2}, \end{aligned} \quad (12)$$

where ω_{rf} is the light-shift-field modulation frequency. By substituting Eq. (12) into Eq. (11), we get the total Stark-shift Hamiltonian:

$$\hat{H}_{LS} = \frac{\hbar(\Omega_{LS}^m)^2}{\Delta} [K_1 |\cos(\omega_{rf} t)| + K_2 \cos(\omega_{rf} t)], \quad (13)$$

where Ω_{LS}^m is the amplitude of the modulated Rabi frequency. The first term is an unwanted perturbation caused by light shift beam. The second term describe a pure fictitious RF field $B_{\text{fict}} \propto I_0 \cos(\omega_{rf} t)$ which is used to perform all-optical spin locking.

D. Optical Rotation Signal

Let us assume that probe light linearly polarized along \hat{x} with detuning δ_{pr} and Rabi frequency Ω_{pr} is used to measure the atomic state of Cs during its evolution. The propagation direction \hat{y} of probe is perpendicular to both the propagation direction of the pump light \hat{x} and the direction of leading field \hat{z} . The pump field with central detuning δ_p and Rabi frequency Ω_p is periodically modulated with frequency Ω_m . To simplify the calculation, we assume here that the frequency of pump is sinusoidally modulated with modulation amplitude Δ_m .

When $\Omega_m = \omega_{rf}$, we can solve the time-periodic evolution equation using Floquet theory [36, 37]. Results of numerical calculations with the AtomicDensityMatrix

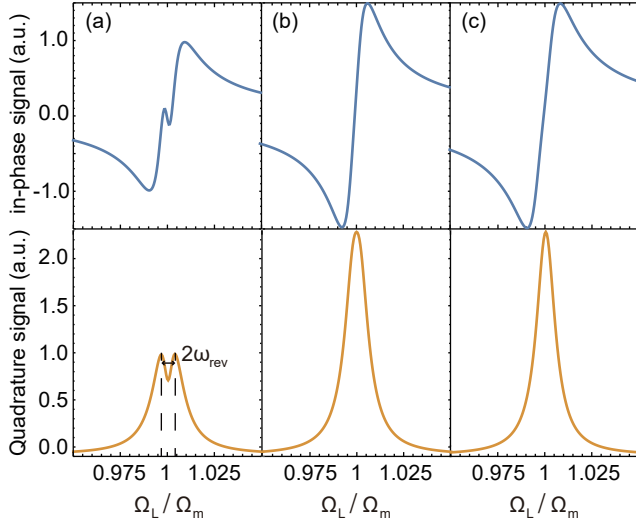


FIG. 2. Theoretical calculated in-phase (top row) and quadrature (bottom row) first-harmonic amplitudes of optical rotation signal. The NLZ effect splits the magnetic resonance into two peaks (a); with the rf spin locking field (b) or intensity modulated light-shift field (c), the spin is locked and magnetic resonance has only one peak. For these plots, the parameters $\Omega_{pr}/\gamma = 100$, $\delta_{pr}/\gamma = 10^6$, $\Omega_p/\gamma = 10^4$, $\delta_p/\gamma = 10^3$, $\Delta_m/\gamma = 10^3$, $\omega_{rev}/\gamma = 1.5$, $\Omega_{rf}/\gamma = 0.02$, $\Omega_{LS}^m/\gamma = 0.02$, $\Delta/\gamma = 10^5$ are chosen.

(ADM) package [31, 38] are shown in Fig. 2 to illustrate the in-phase and quadrature first-harmonic amplitudes of the optical-rotation signal. Here, we consider each sublevel to undergo relaxation (for example, due to spin-depolarizing collisions) at a rate γ . In addition, the upper state undergoes spontaneous decay at a rate $\Gamma = 10^6\gamma$. Without the light-shift beam [Fig. 2(a)], the magnetic resonance is split due to the NLZ effect. Figures 2(b) and (c) show the magnetic resonance with RF field and amplitude-modulated light-shift field, respectively. Up to now, we show the theoretical simulation of all-optical spin locking in $F=1$ to $F'=0$ system. For a real atomic system, there are many hyperfine levels that need to be taken into account for modeling it, which would increase the computational complexity. The results of the real Cs system are shown through the experiments (see Sec:IV).

III. EXPERIMENTAL APPARATUS

Figure 3 shows the experimental apparatus. A paraffin-coated cylindrical cell [39–42] with a length of 5 cm and a diameter of 4 cm containing ^{133}Cs at room temperature, is enclosed within a four-layer mu-metal magnetic shield. The long spin-coherence time in paraffin-coated cell leads to spatial averaging of the optical pumping, probing and stark shift over the en-

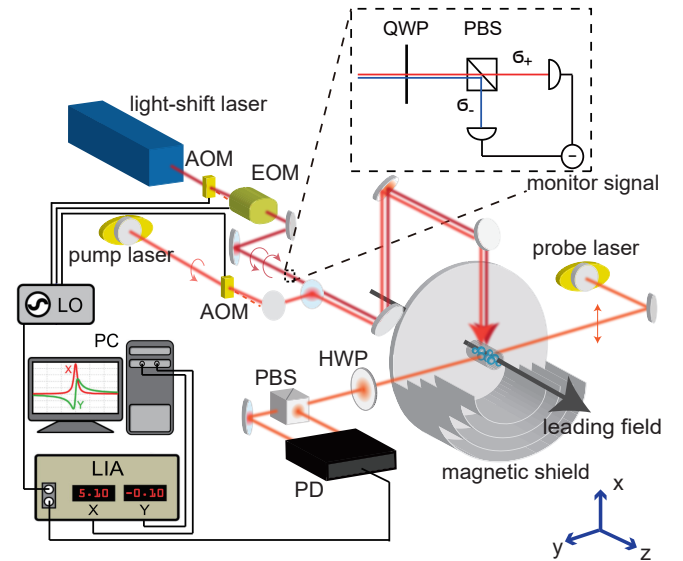


FIG. 3. Experimental setup. AOM: acousto-optic modulator; EOM: electro-optic modulator; HWP: half-wave plate; QWP: Quarter-wave plate; PBS: polarizing beam splitter; PD: balanced photodetector; LIA: lock-in amplifier; LO: local oscillator. A partial view of the magnetic shield is shown in the figure. Atoms are contained in a glass cell positioned in the center of the magnetic shield and are pumped (along $-\hat{x}$) and probed (along \hat{y}) by laser beams under a static magnetic field (along \hat{z}). The intensity of the light-shift laser beam is sinusoidally modulated with an AOM at a frequency Ω_m , while its polarization is switched between the σ_+ and σ_- states every π/Ω_m , using an EOM. Inset shows the monitor setup for polarization and amplitude of the light-shift beam.

tire cell volume [30]. The atoms are prepared in the stretched state along the $-\hat{x}$ direction by optical pumping with a circularly polarized, $-\hat{x}$ -directed laser beam [43, 44]. The pump-laser frequency is locked to the Cs D2 $6^2S_{1/2} F=3 \rightarrow 6^2P_{3/2} F'=4$ transition at 852 nm with a dichroic atomic vapor laser lock (DAVLL) [45]. The beam is pulsed (3% duty cycle) with an acousto-optic modulator (AOM). The light power during the “on” part of the cycle is 50 μW . The polarization rotation of a 10 μW , \hat{y} -directed probe beam induced by the polarized atomic vapor is measured with a balanced polarimeter upon transmission through the cell. The beam is linearly polarized along the x axis and detuned by about 4 GHz towards higher frequencies from the D2 $F=4 \rightarrow F'=5$ transition. A circularly polarized light-shift beam produced with a Ti:sapphire laser propagates parallel to the pump beam. The intensity of the beam is modulated with an AOM and its polarization is modulated with an EOM in order to provide a time-varying light shift. The setup for monitoring the modulation of the light-shift beam is shown in the inset of Fig. 3. A quarter-wave plate is used to convert the circular σ_+ and σ_- components into orthogonal linear polarization components the intensities of which are monitored with two photodetectors. The waist of the collimated laser beam in the vapor cell is

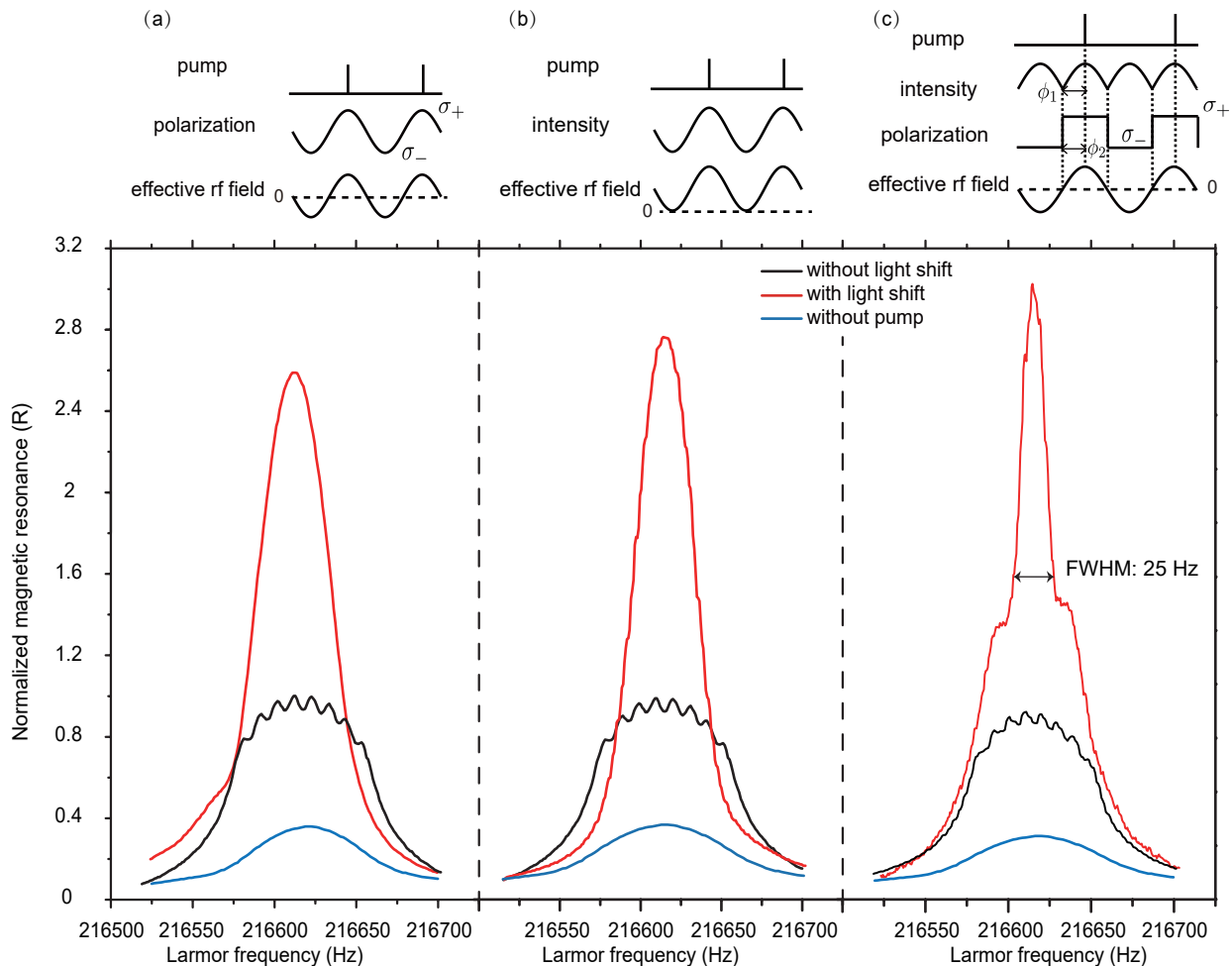


FIG. 4. Magnetic-resonance line shape for a modulation frequency of 216,620 Hz as a function of the leading magnetic field along the z axis with applied light-shift field and pump (red line), without light-shift field (black line), and without pump field (blue line). The amplitude of magnetic resonance without light shift is normalized to unity. The power in (a) and maximum power in (b,c) of the light-shift beam is 200 mW. The inset shows the polarization modulation (a), intensity modulation (b) and both modulated (c) schemes for the pump and light-shift field.

1.5 mm. The frequency of this laser can be widely tuned and is, for most of the experiments presented here, detuned by 10 GHz from the $6^2S_{1/2} F = 4 \rightarrow 6^2P_{3/2} F' = 5$ D2 transition towards lower frequencies. Its frequency is stabilized to the internal reference cavity of the laser. The detuning of 10 GHz was chosen to minimize optical pumping by the light-shift beam while maintaining sufficient fictitious magnetic field amplitude (~ 14 nT for 250 mW power) for spin locking.

To measure the magnetic resonance, we fix the modulation frequency Ω_m of both pump and light-shift beams at a particular value (corresponding to the Larmor frequency for a magnetic field of up to 100 μ T). We scan the leading \hat{z} -directed magnetic field and observe the polarization of the probe beam. The signal from the balanced polarimeter is fed into a lock-in amplifier and demodulated at the modulation frequency. The magnetic resonance can be observed in the polarization rotation amplitude and phase of the probe beam [46].

IV. EXPERIMENTAL RESULTS

We employed three different methods to modulate the light-shift beam and achieve spin locking. Figure 4 shows the amplitude of the lock-in output as a function of the leading magnetic field around 60 μ T with the pump-laser modulation frequency fixed at 216,620 Hz. The magnetic resonance spectra are shown without and with application of the light-shift beam (black and red curves, respectively), as well as without the pump beam (blue curve).

In the method depicted in Fig. 4(a,b), either the intensity or the polarization of the light-shift beam is modulated, to provide a sine-modulated light shift, as in Refs. [29, 32]. In the polarization-modulation scheme, the fictitious magnetic field is oscillating around zero. However, in this scheme, the light is only purely circularly polarized when $\epsilon = \pm 1$; the presence of the other polarizations causes tensor-light shifts that broaden the

transition. In the amplitude-modulation scheme, the VLS produces a fictitious magnetic field of magnitude $B_{\text{fict}} \propto [1 + \cos(\Omega_m t)]$. The oscillating term of the fictitious field locks the spins. The static term of the fictitious field plays no role in spin locking but the constant light leads to broadening of the line width due to residual optical pumping and heading error. In the absence of the light-shift beam, the magnetic resonance is split into eight partially-resolved Lorentzian peaks, due to the NLZ effect. Applying the modulated light-shift beam results in a narrower full-width-half-maximum (FWHM) central peak and an amplitude increase.

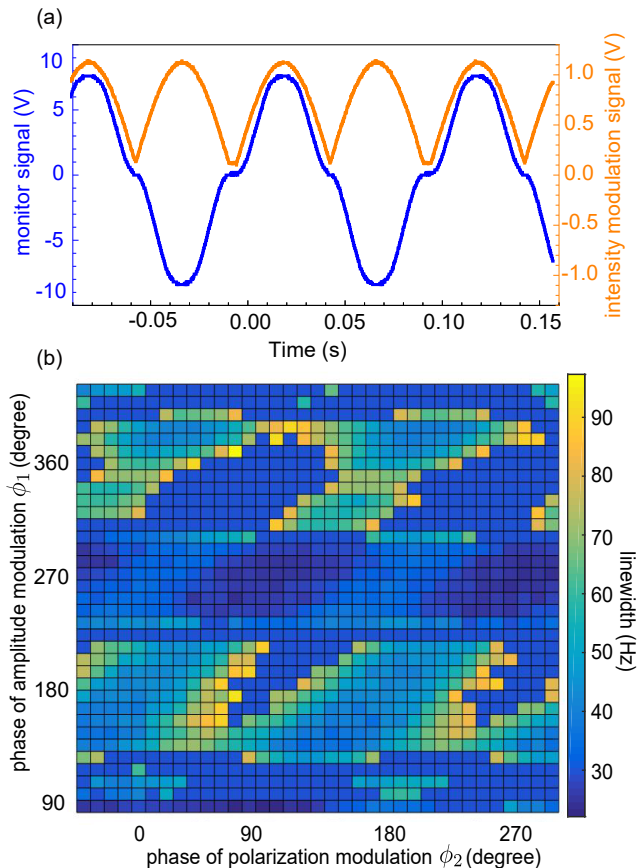


FIG. 5. (a) Observed monitor signal and input intensity modulation signal. Here $\phi_1 = -\pi/2$ and $\phi_2 = -\pi/2$. The distortion of fictitious RF field is mainly caused by nonlinear response of the AOM. (b) Phase scanning of ϕ_1 and ϕ_2 .

In Fig. 4(c), the direction of the fictitious magnetic field is modulated by switching the polarization of the light-shift beam from σ_+ to σ_- using an EOM. In addition, the intensity \mathcal{I} of the light-shift beam is modulated with an AOM as $\mathcal{I} \propto |\cos(\Omega_m t)|$. In this modulation scheme, neglecting the counter-rotating component, the fictitious RF field co-rotates with the precessing spins in the laboratory frame. Since the polarization and propagation direction of light-shift beam and the pump beam are same, the light-shift beam also pump the atoms. The blue lines in Fig. 4 show the magnetic resonance with

light-shift beam while without pump beam. The stochastic nature of the optical pumping leads to a decrease in atomic coherence time and results in a broadening of the magnetic resonance.

The phase of intensity and polarization modulation needs to be chosen carefully to ensure the spin locking field points along the direction of the precessing spins [18]. Firstly, to create a smoothly changing fictitious RF field, the polarization should be switched when the intensity is modulated to zero. Additionally, the fictitious RF field has to be in-phase with the pump pulse. We show the monitor signal (produced by subtraction of the σ_+ and σ_- recorded powers) for $\phi_1 = -\pi/2$ and $\phi_2 = -\pi/2$ in Fig. 5(a), as an fictitious RF field. Here ϕ_1 is the phase of the intensity modulation and ϕ_2 is the phase of the polarization modulation. Figure 5(b) displays the magnetic-resonance line width for different ϕ_1 and ϕ_2 . The best results are achieved around (combinations of) $\phi_1 = \pi/2, 3\pi/2$ and $\phi_2 = \pi/2, 3\pi/2$.

Figure 6 shows the effective line width of the magnetic resonance in Earth-field range (60 μT) as a function of the applied light-shift beam power and detuning. When the light-shift beam is of low power and detuned far off resonance, there is no spin locking and the effective line width is ≈ 100 Hz. When the light-shift beam is near resonance with the atomic transition, the effect of optical pumping is much stronger than that of the VLS. As a result, the line width of the magnetic resonance is even broader than that observed in the absence of the light-shift beam. When the light is far-off resonant from the optical transition, the optical pumping is negligible and the VLS dominates the interaction. We observe a minimum of the line width for a 220 mW light-shift beam, 10 GHz detuned below the D2 $6^2S_{1/2} F = 4 \rightarrow 6^2P_{3/2} F' = 5$ transition. Note, however, that spin locking works well also for the opposite sign of detuning, corresponding to a sign reversal of the effective RF field. The power applied was limited by the available laser.

V. CONCLUSION

We have demonstrated an all-optical method to suppress the NLZ effect in the range of the Earth's magnetic field using spin locking. A polarization and intensity modulated light-shift beam is applied which effectively suppresses NLZ-related broadening of the magnetic resonance. The method works with individual application of intensity or polarization modulation but the combination of both yields the best result. In contrast to other techniques, this method does not cause any crosstalk in sensor networks and also does not interact with samples close to the sensor. The Larmor frequency induced by the optimally effective spin-locking field in the rotating frame is one order of magnitudes larger than spin-revival frequency; the phases (ϕ_1 and ϕ_2) are chosen such that the co-rotating part of the fictitious rf magnetic field is colinear with the precessing spins. We note

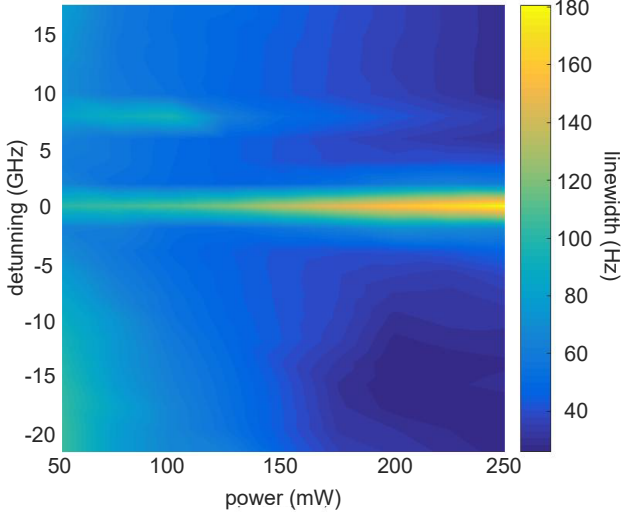


FIG. 6. Map of the magnetic resonance line width as a function of the applied light-shift-field power and detuning. The minimum line width is 25.25(6) Hz.

that the method improves the sensitivity of Earth-field-range magnetometers for two reasons: the increase in the magnetic-resonance signal amplitude and the reduction in the effective line width. We observe some line-width broadening due to residual optical pumping by the light-shift beam, which could be ameliorated using increased optical detuning and higher power. The area of the magnetic resonance profile with both pump and light shift beam is larger than the sum of the profile areas corresponding with only pump or light shift beam. This effect might arise from pumping and repumping by the light shift beam and needs to be further studied. We also note that while the amplitudes of the resonances shown from left to right in Fig. 4 are increasing, the same increase of noise is observed. The measured noise is dominated by magnetic noise due to fluctuations in the current source of leading field.

The authors acknowledge useful discussions with Nataniel L. Figueroa and financial support by the German Federal Ministry of Education and Research (BMBF) within the “Quantumtechnologien” program (FKZ 13N14439) and the DFG through the DIP program (FO 703/2-1). G. B. acknowledges support by the China Scholarship Council and the Fellowship of China Postdoctoral Science Foundation (2020TQ0193, 2021M702146). W. Z. acknowledges support by the National Key Research and Development Program of China under Grant No. 2016YFA0302001, the National Natural Science Foundation of China under Grants No. 11654005, the Quantum Information Technology, Shanghai Municipal Science and Technology Major Project under Grant No. 2019SHZDZX01, and also additional support from the Shanghai talent program. K. J. acknowledges support from the UK Quantum Technology Hub in Sensing

and Timing, funded by the Engineering and Physical Sciences Research Council (EPSRC) (EP/T001046/1). This work was supported by the German Federal Ministry of Education and Research (BMBF) within the Quanten-technologien program (Grant No. 13N15064).

Appendix A: Effective Hamiltonian of Stark Shift

The aim of this appendix is to calculate the light shift due to a circularly polarized field that is near-resonant with an $J = 1 \rightarrow J' = 0$ atomic transition. The detuning from atomic resonance is called Δ and we assume the light is σ_+ polarized and propagating along the x-direction. If we use the x-basis $\{|1, -1\rangle_x, |1, 0\rangle_x, |1, +1\rangle_x, |0', 0'\rangle_x\}$, the light is only affecting one transition $|1, -1\rangle_x \leftrightarrow |0', 0'\rangle_x$ due to the selection rule for σ_+ polarized light (see Fig. 7). The dipole interaction $H = -\mathbf{d} \cdot \mathbf{E}(t)$ can be used to describe the interaction between the atom and the light. The Hamiltonian in rotating wave approximation (RWA) with rotating frequency $\omega_0 + \Delta$ is

$$H = \hbar \begin{pmatrix} 0 & 0 & 0 & 0 \\ 0 & 0 & 0 & 0 \\ 0 & 0 & 0 & -\frac{\Omega_R}{2\sqrt{3}} \\ 0 & 0 & -\frac{\Omega_R}{2\sqrt{3}} & -\Delta \end{pmatrix}_x, \quad (\text{A1})$$

where Ω_R is the Rabi frequency and $|\Omega_R|^2$ is proportional to the intensity of the light. The effect of oscillating fields with frequency $2\omega_0 + \Delta$ is ignored by RWA. The energy eigenvalue E_{J,m_J} of this system is:

$$\begin{aligned} E_{1,-1} &= \frac{\hbar}{6}(-3\Delta + \sqrt{9\Delta^2 + 3\Omega_R^2}) \approx \frac{\hbar\Omega_R^2}{12\Delta}, \\ E_{1,0} &= 0, \\ E_{1,1} &= 0, \\ E_{0',0'} &= \frac{\hbar}{6}(-3\Delta - \sqrt{9\Delta^2 + 3\Omega_R^2}) \approx -\frac{\hbar\Omega_R^2}{12\Delta}. \end{aligned} \quad (\text{A2})$$

As the light is detuned from atomic resonance, it is possible to derive an effective Hamiltonian for the ground states only. In the x -basis for the ground states $\{|1, -1\rangle_x, |1, 0\rangle_x, |1, +1\rangle_x\}$, this Hamiltonian reads

$$H_{\text{eff}} = \frac{\hbar\Omega_R^2}{12\Delta} \begin{pmatrix} 1 & 0 & 0 \\ 0 & 0 & 0 \\ 0 & 0 & 0 \end{pmatrix}_x \quad (\text{A3})$$

We are now interested in finding the Hamiltonian in the z -basis. In order to do so, we notice that a $\pi/2$ rotation about the y -axis rotates the x -axis into the z -axis. This rotation matrix can be written as

$$R(\hat{y}, \pi/2) = \exp\left[-i\left(\frac{\pi}{2}\right)\hat{J}_y\right] = \begin{pmatrix} \frac{1}{2} & -\frac{1}{\sqrt{2}} & \frac{1}{2} \\ \frac{1}{\sqrt{2}} & 0 & -\frac{1}{\sqrt{2}} \\ \frac{1}{2} & \frac{1}{\sqrt{2}} & \frac{1}{2} \end{pmatrix}_x, \quad (\text{A4})$$

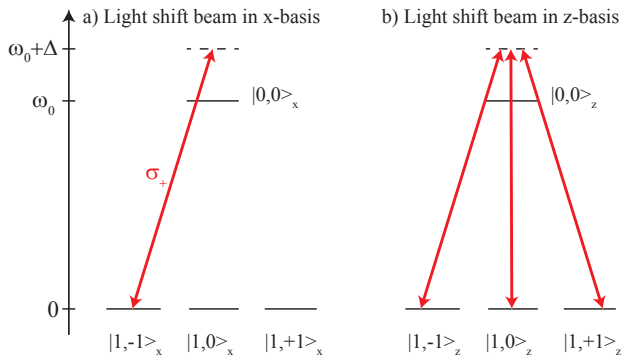


FIG. 7. (a) Schematics for atomic levels $J = 1$ and $J' = 0$ coupled by circular polarized light propagating in the x -direction. Only two levels are coupled in the x -basis. (b) All levels are coupled if one used the z -basis.

We can now find the effective Hamiltonian in the z -basis as

$$\hat{H}_{eff}^+ = R(\hat{y}, \pi/2) H_{eff} R(\hat{y}, \pi/2)^\dagger = \frac{\hbar\Omega_R^2}{12\Delta} \begin{pmatrix} \frac{1}{4} & -\frac{1}{2\sqrt{2}} & \frac{1}{4} \\ -\frac{1}{2\sqrt{2}} & \frac{1}{2} & -\frac{1}{2\sqrt{2}} \\ \frac{1}{4} & -\frac{1}{2\sqrt{2}} & \frac{1}{4} \end{pmatrix}_z. \quad (\text{A5})$$

For σ_- polarized light, the effective Hamiltonian in the z -basis is:

$$\hat{H}_{eff}^- = \frac{\hbar\Omega_R^2}{12\Delta} \begin{pmatrix} \frac{1}{4} & \frac{1}{2\sqrt{2}} & \frac{1}{4} \\ \frac{1}{2\sqrt{2}} & \frac{1}{2} & \frac{1}{2\sqrt{2}} \\ \frac{1}{4} & \frac{1}{2\sqrt{2}} & \frac{1}{4} \end{pmatrix}_z. \quad (\text{A6})$$

With this we arrive at the effective Hamiltonian in the form of Eq. (9) of the main text.

-
- [1] H. Dang, A. Maloof, and M. Romalis, *Appl. Phys. Lett.* **97**, 151110 (2010).
- [2] G. Vasilakis, J. M. Brown, T. W. Kornack, and M. V. Romalis, *Phys. Rev. Lett.* **103**, 261801 (2009).
- [3] I. Altarev *et al.*, *Phys. Rev. Lett.* **103**, 081602 (2009).
- [4] G. Bison, N. Castagna, A. Hofer, P. Knowles, J.-L. Schenker, M. Kasprzak, H. Saudan, and A. Weis, *Appl. Phys. Lett.* **95**, 173701 (2009).
- [5] C. N. Johnson, P. D. D. Schwindt, and M. Weisend, *Phys. Med. Biol.* **58**, 6065 (2013).
- [6] E. Boto *et al.*, *Nature* **555**, 657 (2018).
- [7] R. Zhang *et al.*, *Science Advances* **6**, eaba8792 (2020).
- [8] D. Budker and M. Romalis, *Nature Physics* **3**, 227 (2007).
- [9] S. J. Smullin, I. M. Savukov, G. Vasilakis, R. K. Ghosh, and M. V. Romalis, *Phys. Rev. A* **80**, 033420 (2009).
- [10] M. P. Ledbetter, I. M. Savukov, V. M. Acosta, D. Budker, and M. V. Romalis, *Phys. Rev. A* **77**, 033408 (2008).
- [11] W. C. Griffith, S. Knappe, and J. Kitching, *Opt. Express* **18**, 27167 (2010).
- [12] V. Acosta, M. P. Ledbetter, S. M. Rochester, D. Budker, D. F. Jackson Kimball, D. C. Hovde, W. Gawlik, S. Pustelny, J. Zachorowski, and V. V. Yashchuk, *Phys. Rev. A* **73**, 053404 (2006).
- [13] S. J. Seltzer, P. J. Meares, and M. V. Romalis, *Phys. Rev. A* **75**, 051407 (2007).
- [14] V. Acosta, M. Auzinsh, W. Gawlik, P. Grisins, J. Higbie, D. J. Kimball, L. Krzemien, M. Ledbetter, S. Pustelny, S. Rochester, *et al.*, *Optics Express* **16**, 11423 (2008).
- [15] K. Jensen, V. M. Acosta, J. M. Higbie, M. P. Ledbetter, S. M. Rochester, and D. Budker, *Phys. Rev. A* **79**, 023406 (2009).
- [16] W. Li, X. Peng, S. Li, C. Liu, H. Guo, P. Lin, and W. Zhang, in *Frequency Control Symposium (IFCS), 2016 IEEE International* (IEEE, 2016) pp. 1–4.
- [17] W. Chalupczak, A. Wojciechowski, S. Pustelny, and W. Gawlik, *Physical Review A* **82**, 023417 (2010).
- [18] G. Bao, A. Wickenbrock, S. Rochester, W. Zhang, and D. Budker, *Phys. Rev. Lett.* **120**, 033202 (2018).
- [19] G. Lembke, S. N. Erné, H. Nowak, B. Menhorn, A. Pasquarelli, and G. Bison, *Biomed. Opt. Express* **5**, 876 (2014).
- [20] S. Groeger, G. Bison, and A. Weis, *Journal of research of the National Institute of Standards and Technology* **110**, 179 (2005).
- [21] E. Aleksandrov, M. Balabas, S. Dmitriev, *et al.*, *Tech. Phys. Lett.* **32**, 627 (2006).
- [22] A. Borna, T. R. Carter, J. D. Goldberg, A. P. Colombo, Y.-Y. Jau, C. Berry, J. McKay, J. Stephen, M. Weisend, and P. D. Schwindt, *Phys. Med. Biol.* **62**, 8909 (2017).
- [23] J. M. Higbie, S. M. Rochester, B. Patton, R. Holzlöhner, D. B. Calia, and D. Budker, *Proceedings of the National Academy of Sciences* **108**, 3522 (2011).
- [24] B. Patton, O. Versolato, D. C. Hovde, E. Corsini, J. M. Higbie, and D. Budker, *Appl. Phys. Lett.* **101**, 083502 (2012).
- [25] F. P. Bustos, D. B. Calia, D. Budker, M. Centrene, J. Hellemeier, P. Hickson, R. Holzlöhner, and S. Rochester, *arXiv preprint arXiv:1802.04686* (2018).
- [26] B. S. Mathur, H. Tang, and W. Happer, *Phys. Rev.* **171**, 11 (1968).
- [27] C. Cohen-Tannoudji and J. Dupont-Roc, *Phys. Rev. A* **5**, 968 (1972).
- [28] F. Le Kien, P. Schneeweiss, and A. Rauschenbeutel, *The European Physical Journal D* **67**, 92 (2013).
- [29] B. Patton, E. Zhivun, D. C. Hovde, and D. Budker, *Phys. Rev. Lett.* **113**, 013001 (2014).
- [30] E. Zhivun, A. Wickenbrock, J. Sudyka, B. Patton, S. Pustelny, and D. Budker, *Opt. Express* **24**, 15383 (2016).
- [31] M. Auzinsh, D. Budker, and S. Rochester, *Optically polarized atoms: understanding light-atom interactions* (Oxford University Press, 2010).
- [32] E. Zhivun, A. Wickenbrock, B. Patton, and D. Budker, *Appl. Phys. Lett.* **105**, 192406 (2014).
- [33] Z. Lin, X. Peng, W. Li, H. Wang, and H. Guo, *Opt. Express* **25**, 7668 (2017).
- [34] G. Breit and I. I. Rabi, *Phys. Rev.* **38**, 2082 (1931).
- [35] B. Julsgaard, *Entanglement and quantum interactions*

- with macroscopic gas samples*, Ph.D. thesis, Aarhus Universitetsforlag (2003).
- [36] S. M. Rochester, *Modeling nonlinear magneto-optical effects in atomic vapors*, Ph.D. thesis, UC Berkeley (2010).
- [37] S. Coop, S. Palacios, P. Gomez, Y. N. M. de Escobar, T. Vanderbruggen, and M. W. Mitchell, *Opt. Express* **25**, 32550 (2017).
- [38] <http://rochesterscientific.com/ADM/>.
- [39] H. Robinson, E. Ensberg, and H. Dehmelt, *Bull. Am. Phys. Soc* **3** (1958).
- [40] M. Bouchiat and J. Brossel, *Phys. Rev.* **147**, 41 (1966).
- [41] E. B. Alexandrov and V. A. Bonch-Bruевич, *Optical Engineering* **31**, 711 (1992).
- [42] E. Alexandrov, M. Balabas, D. Budker, D. English, D. Kimball, C.-H. Li, and V. Yashchuk, *Phys. Rev. A* **66**, 042903 (2002).
- [43] Z. D. Grujić and A. Weis, *Physical Review A* **88**, 012508 (2013).
- [44] S. Li, Y. Zhang, Y. Tian, J. Chen, and S. Gu, *Journal of Applied Physics* **130**, 084501 (2021).
- [45] V. V. Yashchuk, D. Budker, and J. R. Davis, *Review of Scientific Instruments* **71**, 341 (2000).
- [46] D. Budker, W. Gawlik, D. F. Kimball, S. M. Rochester, V. V. Yashchuk, and A. Weis, *Rev. Mod. Phys.* **74**, 1153 (2002).